The Prediction of Jet Noise Ground Effects using an Acoustic Analogy and a Tailored Green's Function

Steven A. E. Miller*

The National Aeronautics and Space Administration

An assessment of an acoustic analogy for the mixing noise component of jet noise in the presence of an infinite surface is presented. The reflection of jet noise by the ground changes the distribution of acoustic energy and is characterized by constructive and destructive interference patterns. The equivalent sources are modeled based on the two-point cross-correlation of the turbulent velocity fluctuations and a steady Reynolds-Averaged Navier-Stokes (RANS) solution. Propagation effects, due to reflection by the surface and refraction by the jet shear layer, are taken into account by calculating the vector Green's function of the linearized Euler equations (LEE). The vector Green's function of the LEE is written in relation to Lilley's equation; that is, approximated with matched asymptotic solutions and the Green's function of the convective Helmholtz equation. The Green's function of the convective Helmholtz equation for an infinite flat plane with impedance is the Weyl-van der Pol equation. Predictions are compared with an unheated Mach 0.95 jet produced by a nozzle with an exit diameter of 0.3302 meters. Microphones are placed at various heights and distances from the nozzle exit in the peak jet noise direction above an acoustically hard and an asphalt surface. The predictions are shown to accurately capture jet noise ground effects that are characterized by constructive and destructive interference patterns in the mid- and far-field and capture overall trends in the near-field.

Nomenclature

A_s	Constant associated with dilatation source
B_s	Constant associated with unsteady force per unit volume source
c	Speed of sound
c_l	Constant of integral length scale
c_u	Constant of integral velocity scale
c_τ	Constant of integral time scale
D	Nozzle exit diameter
E	Variation of two-point cross-correlation of velocity fluctuations with space and time
F	Rudwick boundary loss factor
f	Frequency
f_i	Unsteady force per unit volume associated with velocity fluctuations
g	Green's function of the convective Helmholtz equation
g_l	Green's function of Lilley's equation
g_o^*	Location of turning point
K	Turbulent kinetic energy
l_x	Integral length scale in the streamwise direction
l_y	Integral length scale in the y direction
l_z	Integral length scale in the z direction
M	Mach number
M_j	Fully expanded Mach number
p	Pressure
R_p	Reflection coefficient
R_s	Flow resistivity
r	Radial direction
S	Spectral density
TTR	Total temperature ratio
t	Time

*Research Aerospace Engineer, Aeroacoustics Branch, NASA Langley Research Center, 2 N. Dryden St. MS 461, Hampton, VA, 23681, USA, AIAA Member, s.miller@nasa.gov

u	Streamwise velocity component in the x direction
u_s	Integral scale of velocity
v	Radial velocity component in the y direction
w	Radial velocity component in the z direction or numerical distance
$\boldsymbol{x}$	Observer position
x	Streamwise direction
$\boldsymbol{y}$	Source position
$\boldsymbol{z}$	Vector from source to observer
z_s	Surface impedance
γ	Ratio of specific heats
δ	Dirac delta function
ϵ	Dissipation rate of turbulent kinetic energy
$\boldsymbol{\eta}$	Vector between two source locations (ξ, η, ζ)
θ	Dilatation rate or observer angle from nozzle downstream axis
π	Logarithm of the pressure
π_g^n	Vector Green's function of the linearized Euler equations
ρ	Density
τ	Retarded time
τ_s	Integral time scale
ϕ	Azimuthal angle
Ψ	Observer angle from the nozzle inlet axis
Ω	Specific dissipation rate of turbulent kinetic energy
ω	Radian frequency
Subscript	
j	Jet fully expanded quantity
p	Property of the primary jet
s	Property of turbulence
∞	Ambient value

Introduction

An acoustic analogy is developed based on the Euler equations for the prediction of jet mixing noise in the vicinity of an arbitrary geometry. The analogy is based on the development by Morris and Farassat[1] but has unique differences. The Euler equations, written in terms of the logarithm of the pressure, are rearranged into a left hand side operator consistent with the linearized Euler equations (LEE) and right hand side equivalent sources. The far-field pressure is written in terms of an integral solution of the governing equations. It appears as a volumetric integral of the equivalent sources and the vector Green's function of the LEE. Any adjoint vector Green's function solver for the LEE can be used within the analogy. Equivalent source models are created for both the dilatation and unsteady force per unit volume source terms. The equivalent sources follow the models of Tam and Auriault[2] & Morris and Boluriaan.[3] The model is dependent on steady Reynolds-Averaged Navier-Stokes (RANS) solutions but could easily be based on an empirical flow-field or unsteady simulation. This allows the nozzle pressure ratio, temperature ratio, and nozzle geometry to be connected directly to the aerodynamic solution and resultant jet noise. A model of the two-point cross-correlation of the unsteady velocity fluctuations within the jet connects the turbulence statistics to the prediction. It is based on measurement and the turbulence statistics generated by a two-equation closure of the steady RANS equations.

The refraction of the sound through the meanflow, diffraction by surfaces, or reflection by the ground or airframe, are all handled by the solution of the vector Green's function of the LEE. For simplicity in this investigation, the vector Green's function of the LEE is written in terms of Lilley's[4] equation. An approximate solution of Lilley's equation is formed about the Green's function of the convective Helmholtz equation. Analytic forms of the Green's function of the convective Helmholtz equation are used to account for sound reflection on an infinite flat surface which is representative of the ground. The impedance model of Delany and Bazley[5] is used to simulate the damping of the reflected acoustic waves, but can be neglected for an acoustically hard wall. The form of the Green's function of the convective Helmholtz equation is the Weyl-van der Pol[6] formula. The geometry chosen to exercise the model coincides with the experiment by Miles.[7]

The methodology presented in this paper is developed to address many of the issues encountered by previous investigators. Experimental measurements conducted near reflecting surfaces pose unique difficulties. These are summarized well by the studies of Seiner *et al.*,[8] Butzel,[9] Schlinker *et al.*,[10] Pao *et al.*,[11] Huber and Sogeti,[12] and many others, who performed experiments with microphones at or near various surface

locations relative to static jet and aircraft flyover. With careful microphone placement and corrections, accurate measurements can be conducted.

A large body of prediction methodologies were developed to address reflection and impedance effects. In particular, Illston *et al.*[13] performed a combined theoretical and experimental study on jet noise, erosion, and ground effects. Their methodology used a Harper-Bourne[14] like prediction approach by integrating the source strength per unit length along the centerline jet axis. The Aircraft Noise Prediction Program (ANOPP) (see Zorumski[15] for details), accounts for ground effects from various sources such as the fan, jet, and airframe. ANOPP uses ground reflection corrections described by Chien and Soroka[16] and the impedance model by Delany and Bazley.[5] Finally, McLaughlin *et al.*[17] performed a series of experiments and predictions using supersonic jets with and without a ground plane. They created a model to describe the source distribution within the jet plume and predictions showed that the interference patterns were correctly predicted at high frequencies.

In the following sections, the model development is presented starting with the governing equations. An overview of the implementation of the method in a computer program, its connection to a steady RANS solver, a description of the model calibration, and method to find the steady RANS solution are shown. Results of the predictions are compared with the experiment of Miles.[7]

Mathematical Model

The acoustic analogy presented herein is based on that of Morris and Farassat.[1] The governing equations are the Euler equations,

$$\frac{D\pi}{Dt} + \frac{\partial u_i}{\partial x_i} = 0 \tag{1}$$

$$\frac{Du_i}{Dt} + c^2 \frac{\partial \pi}{\partial x_i} = 0 \tag{2}$$

where D/Dt is the material derivative, c is the speed of sound, u is the velocity, and $\pi = \gamma^{-1} ln(p/p_\infty)$. By linearizing the governing equations about a non-radiating base-flow and retaining terms on the left hand side that are linear in fluctuation then the inhomogeneous LEE are formed.

$$\frac{\partial \pi'}{\partial t} + \overline{u}_j \frac{\partial \pi'}{\partial x_j} + \frac{\partial u_i'}{\partial x_i} = \theta \tag{3}$$

and,

$$\frac{\partial u_i'}{\partial t} + \overline{u}_j \frac{\partial u_i'}{\partial x_j} + u_j' \frac{\partial \overline{u}_i}{\partial x_j} + \overline{c}^2 \frac{\partial \pi'}{\partial x_i} = f_i \tag{4}$$

where,

$$\theta = -u_j' \frac{\partial \overline{\pi}}{\partial x_j} - u_j' \frac{\partial \pi'}{\partial x_j} \tag{5}$$

is a dilatation rate and,

$$f_i = -c^{2'} \frac{\partial \overline{\pi}}{\partial x_i} - c^{2'} \frac{\partial \pi'}{\partial x_i} - u_j' \frac{\partial u_i'}{\partial x_j} \tag{6}$$

is a unsteady force per unit mass. In both the equivalent sources only the second order fluctuations are considered to contribute to the sound field. Note that $\pi' \simeq \gamma^{-1} ln(1 + p'/p_\infty) \simeq \gamma^{-1} p'/p_\infty$. The vector Green's function of the LEE is defined as,

$$\frac{D_o \pi_g^n}{Dt} + \frac{\partial u_{gi}^n}{\partial x_i} = \delta(\boldsymbol{x} - \boldsymbol{y}) \delta(t - \tau) \delta_{0n} \tag{7}$$

and

$$\frac{D_o u_{gi}^n}{Dt} + u_{gj}^n \frac{\partial \overline{u}_i}{\partial x_j} + \overline{c}^2 \frac{\partial \pi_g^n}{\partial x_i} = \delta(\boldsymbol{x} - \boldsymbol{y}) \delta(t - \tau) \delta_{in}. \tag{8}$$

where $D_o/Dt = \partial/\partial t + \overline{u}_j \partial/\partial x_j$. Let the vector Green's function be periodic,

$$\pi_g^n(\boldsymbol{x}, t|\boldsymbol{y}, \tau) = \int_{-\infty}^{\infty} \pi_g^n(\boldsymbol{x}|\boldsymbol{y}; \omega) \exp[i\omega(t-\tau)] d\omega \tag{9}$$

and

$$\pi_g^n(\boldsymbol{x}|\boldsymbol{y}; \omega) = \frac{1}{2\pi} \int_{-\infty}^{\infty} \pi_g^n(\boldsymbol{x}, t|\boldsymbol{y}, \tau) \exp[-i\omega(t-\tau)] d\tau. \tag{10}$$

The fluctuating far-field pressure is a convolution integral of the vector Green's function and the equivalent sources,

$$p'(\boldsymbol{x}, t) = \gamma p_\infty \int_{-\infty}^{\infty} ... \int_{-\infty}^{\infty} \pi_g^0(\boldsymbol{x}, t|\boldsymbol{y}, \tau)\theta(\boldsymbol{y}, \tau) + \sum_{n=1}^{3} \pi_g^n(\boldsymbol{x}, t|\boldsymbol{y}, \tau) f_n(\boldsymbol{y}, \tau) d\tau d\boldsymbol{y}. \tag{11}$$

The spectral density is defined as the Fourier transform of the autocorrelation of the fluctuating pressure,

$$S(\boldsymbol{x}, \omega) = \int_{-\infty}^{\infty} \overline{p'(\boldsymbol{x}, t) p'(\boldsymbol{x}, t+\tau)} \exp[-i\omega\tau] d\tau. \tag{12}$$

Using Eqns. 11 and 12 yields,

$$\begin{aligned} S(\boldsymbol{x}, \omega) = \rho_\infty^2 c_\infty^4 \int_{-\infty}^{\infty} ... \int_{-\infty}^{\infty} \{ & \pi_g^0(\boldsymbol{x}, \boldsymbol{y}, -\omega) \pi_g^0(\boldsymbol{x}, \boldsymbol{y}+\boldsymbol{\eta}, \omega) \overline{\theta(\boldsymbol{y}, \tau)\theta(\boldsymbol{y}+\boldsymbol{\eta}, t+\tau)} \\ + \sum_{n=1}^{3} \sum_{m=1}^{3} & \pi_g^n(\boldsymbol{x}, \boldsymbol{y}, -\omega) \pi_g^m(\boldsymbol{x}, \boldsymbol{y}+\boldsymbol{\eta}, \omega) \overline{f_n(\boldsymbol{y}, \tau) f_m(\boldsymbol{y}+\boldsymbol{\eta}, t+\tau)} \} \exp[-i\omega\tau] d\tau d\boldsymbol{\eta} d\boldsymbol{y}. \end{aligned} \tag{13}$$

By definition the periodic vector Green's function of the LEE,

$$\pi_g^{n*}(\boldsymbol{x}, \boldsymbol{y}, \omega) = \pi_g^n(\boldsymbol{x}, \boldsymbol{y}, -\omega) \tag{14}$$

and following Tam and Auriault,[2] two closely placed source points in the jet are related by,

$$\pi_g^n(\boldsymbol{x}, \boldsymbol{y}+\boldsymbol{\eta}, \omega) \simeq \pi_g^n(\boldsymbol{x}, \boldsymbol{y}, \omega) \exp\left[\frac{-i\omega\xi}{c_\infty} \cos\theta\right]. \tag{15}$$

Using Eqns. 14 and 15 with Eqn. 13 yields,

$$\begin{aligned} S(\boldsymbol{x}, \omega) = \rho_\infty^2 c_\infty^4 \int_{-\infty}^{\infty} ... \int_{-\infty}^{\infty} \{ & \pi_g^{*0}(\boldsymbol{x}, \boldsymbol{y}, \omega) \pi_g^0(\boldsymbol{x}, \boldsymbol{y}, \omega) \overline{\theta(\boldsymbol{y}, \tau)\theta(\boldsymbol{y}+\boldsymbol{\eta}, t+\tau)} \\ + \sum_{n=1}^{3} \sum_{m=1}^{3} & \pi_g^{*n}(\boldsymbol{x}, \boldsymbol{y}, \omega) \pi_g^m(\boldsymbol{x}, \boldsymbol{y}, \omega) \overline{f_n(\boldsymbol{y}, \tau) f_m(\boldsymbol{y}+\boldsymbol{\eta}, t+\tau)} \} \exp\left[\frac{-i\omega\xi}{c_\infty} \cos\theta\right] \exp[-i\omega\tau] d\tau d\boldsymbol{\eta} d\boldsymbol{y}. \end{aligned} \tag{16}$$

We have now obtained a general formulation that involves the two-point cross-correlation of the equivalent sources and the vector Green's function of the LEE. A model is required for the two-point cross-correlation of the equivalent sources and the vector Green's function of the LEE.

The dilatation rate source is modeled following Tam and Auriault[2] and written in the form of Morris and Boluriaan,[3]

$$\overline{\theta(\boldsymbol{y}, \tau)\theta(\boldsymbol{y}+\boldsymbol{\eta}, t+\tau)} = A_s^2 \frac{(u_s/c_\infty)^4}{\tau_s^2} E(\boldsymbol{\eta}, \tau) \tag{17}$$

where A_s is a constant. The two-point cross-correlation of the unsteady force per unit volume is modeled following Morris and Boluriaan,[3]

$$\overline{f_n(\boldsymbol{y}, \tau) f_m(\boldsymbol{y}+\boldsymbol{\eta}, t+\tau)} = B_s^2 \frac{(u_s/c_\infty)^2 u_s^4}{l_x^2} E(\boldsymbol{\eta}, \tau) \tag{18}$$

where B_s is a constant. A model must be formed for the space-time decay function $E(\boldsymbol{\eta}, \tau)$. Following Ribner's[18] postulate, the spatial and temporal terms of $E(\boldsymbol{\eta}, \tau)$ are separable,

$$E(\boldsymbol{\eta}, \tau) = \exp\left[\frac{-|\tau|}{\tau_s}\right] \exp\left[\frac{-(\xi - \overline{u}\tau)^2}{l_x^2}\right] \exp\left[\frac{-(\eta - \overline{v}\tau)^2}{l_y^2}\right] \exp\left[\frac{-(\zeta - \overline{w}\tau)^2}{l_z^2}\right] \tag{19}$$

Equations 17 through 19 are used in Eqn. 16. Integrals involving the variables of integration τ, η, ξ, and ζ are performed analytically. Assumptions required for analytical integration involving $\boldsymbol{\eta}$ and τ require $\tau_s > 0$, $l_i > 0$, $c_\infty > 0$, $x > 0$, and for these quantities to be real. These are reasonable assumptions physically as the turbulent kinetic energy at the boundary is zero and we restrict our modeling of the jet flow where $x = 0$ represents the nozzle exit. These integrations result in,

$$\begin{aligned} S(\boldsymbol{x}, \omega) = \rho_\infty^2 c_\infty^4 \int_{-\infty}^{\infty}\int_{-\infty}^{\infty}\int_{-\infty}^{\infty} & \frac{2\pi^{3/2} c_\infty^2 l_x l_y l_z \tau_s x^2}{c_\infty^2 x^2 + (ux_1 + vx_2 + wx_3 + c_\infty x)^2 \tau_s^2 \omega^2} \\ \times \left\{ \pi_g^{*0}(\boldsymbol{x}, \boldsymbol{y}, \omega) \pi_g^0(\boldsymbol{x}, \boldsymbol{y}, \omega) A_s^2 \frac{(u_s/c_\infty)^4}{\tau_s^2} + \sum_{n=1}^{3}\sum_{m=1}^{3} \pi_g^{*n}(\boldsymbol{x}, \boldsymbol{y}, \omega) \pi_g^m(\boldsymbol{x}, \boldsymbol{y}, \omega) B_s^2 \frac{(u_s/c_\infty)^2 u_s^4}{l_x^2} \right\} & \\ \times \exp\left[-\frac{\left(l_x^2 x_1^2 + l_y^2 x_2^2 + l_z^2 x_3^2\right)\omega^2}{4c_\infty^2 x^2} \right] d\boldsymbol{y}. & \end{aligned} \tag{20}$$

The integral scales of turbulence in Eqn. 20, l_x, l_y, l_z, u_s, and τ_s, are required to make a prediction. These could be found by simple empirical models or unsteady CFD simulations. Here, they are related to a steady RANS solution by,

$$l_x(\boldsymbol{y}) = c_l K(\boldsymbol{y})/\epsilon(\boldsymbol{y}), \tag{21}$$

$$\tau_s(\boldsymbol{y}) = c_\tau K(\boldsymbol{y})/\epsilon(\boldsymbol{y}), \tag{22}$$

and,

$$u_s(\boldsymbol{y}) = c_u \sqrt{2K(\boldsymbol{y})/3}. \tag{23}$$

The coefficients are $c_\tau = 0.30$, $c_u = 1.00$, and $c_l = 1.00$. These coefficients are based on a reference jet operating at the sonic condition, $TTR = 3.20$, and a 0.0508 m convergent nozzle at the sideline location of $R/D = 100$. They have been calibrated by the same methodology of Tam and Auriault.[2] Their variation from Tam and Auriault is attributed to the use of a different acoustic analogy and steady RANS solver. The cross-stream integral length scales, l_y and l_z, are set to 3/10 of l_x, which corresponds to experimental observation. These coefficients are never altered irrespective of the nozzle Mach number, diameter, temperature, nozzle geometry, or any other parameter.

A solution for π_g^n is now required. One method suitable for calculating the vector Green's function of the LEE is by finding the Green's function of Lilley's[4] equation. The vector Green's function of the LEE are related to the Green's function of Lilley's[4] equation by,

$$\pi_g^0(\boldsymbol{x}, \boldsymbol{y}, \omega) = \omega^2 g_l(\boldsymbol{x}, \boldsymbol{y}, \omega) - 2i\overline{u}\omega \frac{\partial g_l(\boldsymbol{x}, \boldsymbol{y}, \omega)}{\partial y_x} - \overline{u}^2 \frac{\partial^2 g_l(\boldsymbol{x}, \boldsymbol{y}, \omega)}{\partial y_x^2} \tag{24}$$

$$\pi_g^1(\boldsymbol{x}, \boldsymbol{y}, \omega) = -\left(i\omega + \overline{u}\frac{\partial}{\partial y_x}\right) \frac{\partial}{\partial y_x} g_l(\boldsymbol{x}, \boldsymbol{y}, \omega) \tag{25}$$

$$\pi_g^2(\boldsymbol{x}, \boldsymbol{y}, \omega) = -\left\{ 3\frac{\partial \overline{u}}{\partial y_r}\frac{\partial}{\partial y_x} - \left(i\omega + \overline{u}\frac{\partial}{\partial y_x}\right)\frac{\partial}{\partial y_r} \right\} g_l(\boldsymbol{x}, \boldsymbol{y}, \omega) \tag{26}$$

$$\pi_g^3(\boldsymbol{x}, \boldsymbol{y}, \omega) = -\left(i\omega + \overline{u}\frac{\partial}{\partial y_x}\right) \frac{1}{y_r}\frac{\partial}{y_\theta} g_l(\boldsymbol{x}, \boldsymbol{y}, \omega) \tag{27}$$

where the subscript of the source vector $\boldsymbol{y}$ denotes the direction the partial derivative is taken. The problem is now reduced to finding the Green's function of Lilley's equation instead of the full vector Green's function of the LEE. Tam and Auriault[19] and Raizada[20] performed this technique with success. These methods used

an adjoint approach and are relatively computationally inexpensive. However, these methods do not include a scattering surface such as the airframe or ground, thus analytic or numerical approximations of Lilley's equation that have the potential to include a scattering surface are sought.

Analytical solutions of Lilley's[4] equation can be found but only for very special mean flows. These are instructive but not helpful for more realistic jets. An asymptotic solution of Lilley's equation for low frequencies was found by Goldstein[21,22,23] and for high frequencies by Balsa *et al.*[24] By examination of the asymptotic solutions, the Green's function of the convective Helmholtz equation, g, and a matching function, an approximate Green's function of Lilley's equation is created,

$$g_l(\boldsymbol{x},\boldsymbol{y},\omega) = \begin{cases} \frac{i}{c_\infty^2 c_0^{c_\alpha}\omega}\frac{c_\infty}{\bar{c}} \exp\left[\frac{-i\omega}{c_\infty}\left(x\cos\theta + r\sin\theta\cos\left(\phi_0-\phi\right)\right)\right] g & \text{if } Re[g_o^*] > 0 \\ \frac{i}{c_\infty^2 c_0^{c_\alpha}\omega}\frac{c_\infty}{\bar{c}} \exp\left[\frac{-i\omega}{c_\infty}\left(x\cos\theta + r\sin\theta\cos\left(\phi_0-\phi\right)\right)\right] \exp\left[-c_\beta\omega/c_\infty\right] g & \text{if } Re[g_o^*] \le 0 \end{cases} \tag{28}$$

where c is the local speed of sound, $c_\beta = 1\times10^{-4}$, and,

$$g_o^* = \sqrt{\frac{(1-\overline{u}/c_\infty\cos\theta)^2}{(\bar{c}^2/c_\infty^2)} - \cos^2\theta}. \tag{29}$$

C_0 is Ribner's convection coefficient,

$$C_0 = \sqrt{(1-\overline{u}/c_\infty\cos\theta)^2 + c_{0\alpha}^2(\overline{u}/c_\infty)^2} \tag{30}$$

where $c_{0\alpha} = (4/25)\sqrt{u_j/c_\infty - 1}$. The convective amplification power coefficient is,

$$c_\alpha = 3 - \tanh\left[fD_j/u_j\right]. \tag{31}$$

The benefit of this approach is existing numerical solvers can provide the Green's function of the convective Helmholtz equation. For example, the Fast Scattering Code (FSC) by Tinetti and Dunn,[25] any Boundary Element Method (BEM) (see an overview by Katsikadelis[26]), or FastBEM by Liu.[27] This permits the opportunity of finding the jet noise scattering from any surface as long as the aerodynamic noise sources are minimally affected by the scattering geometry.

For static jet predictions the Green's function of the Helmholtz equation is used, $g = \exp[ik\boldsymbol{z}]/(4\pi\boldsymbol{z})$. If an infinite plane exists parallel to the jet centerline then the tailored Green's function of the Helmholtz equation is represented by the Weyl-van der Pol[6] formula,

$$g = \frac{\exp[ikz]}{4\pi z} + \left[R_p + (1-R_p)F(w)\right]\frac{\exp[ikR_2]}{4\pi R_2} \tag{32}$$

where R_2 is the distance from an equivalent source point on the opposite side of the infinite plane to the observer and R_p is the reflection coefficient,

$$R_p = \frac{Z_s(f)\cos\theta - \rho_\infty c_\infty}{Z_s(f)\cos\theta + \rho_\infty c_\infty} \tag{33}$$

and $F(w)$ is the Rudwick boundary loss factor,

$$F(w) = 1 + i\sqrt{\pi}w\exp\left[-w^2\right]\operatorname{erfc}\left[-iw\right] \tag{34}$$

where erfc is the complementary error function. We numerically evaluate erfc using the identity $\operatorname{erfc}[-iw] = 1 - \operatorname{erf}[-iw]$. w is the numerical distance,

$$w = \frac{1}{2}(1+i)\sqrt{2\pi f R_2/c_\infty}\left[\cos\theta + (\rho_\infty c_\infty)^{-1}\right]. \tag{35}$$

There are many models for the surface impedance Z_s. Following ANOPP,[15] one appropriate choice is the model of Delany and Bazley,[5]

$$Z_s = \rho_\infty c_\infty\left[1 + 0.0571X(f)^{-0.754} + i0.87X(f)^{-0.732}\right] \tag{36}$$

where $X(f) = \rho_\infty f/R_s$. R_s is the flow resistivity. The asymptotic solution of Z_s for R_s approaching infinity yields the hard-wall solution.

Results

The developed mathematical models are now assessed by comparing them with the experimental measurements of Miles.[7] Here, a convergent nozzle with a 0.3302 m (13 inch) exit diameter was placed in an open environment with the jet centerline axis 3.89 m (12.75 ft) above the ground. The nozzle centerline axis was parallel to the ground. The ground was described as asphalt and has a flow resistivity of $R_s = 27000$ Pa s / m^2, which is the average flow resistively described by Attenborough *et al.*[28] The ambient environment had a temperature of 288.9 K and was described as dry. Corrections have been made for atmospheric absorption. Microphones were placed relative to the nozzle exit at an angle $\psi = 145$ degrees from the upstream axis. Three sets of microphones were located at this observer angle at ground shadow distances (distance from a point on the ground under the nozzle measured to a point under the microphone) of 7.62, 15.24, and 22.86 m. At each of these observer distances, microphones were placed at 0.0061, 1.52, and 3.89 m above the ground. Lossless sound pressure level spectra were calculated in 1/3 octave bands from 50 to 20,000 Hz.

The coordinate system shown in Fig. 1 illustrates the relative positions of the microphones with respect to the nozzle. The nozzle is shown on the left side of the figure and the jet plume develops from the left to right direction along the positive x-axis. The y-axis is normal to the ground and the z-axis is parallel to the ground in the sideline observer direction. The height of the nozzle is specified by the distance along a normal from the ground plane to the center of the nozzle exit. The observer angle, ψ, is the angle from the upstream nozzle centerline axis to the observer. The azimuthal angle, ϕ, is measured about the x-axis originating from the x-y plane. Values of $\boldsymbol{x}$ are specified to find the microphone position relative to the nozzle exit along with the microphone height.

The Steady RANS Solution

The developed prediction model requires the knowledge of a mean flow. The steady RANS solution is found with the Fully Unstructured Navier-Stokes (FUN3D) solver from The NASA Langley Research Center. For more information on FUN3D see Anderson and Bonhaus[29] or Nielsen.[30] The steady RANS equations are closed with the Menter[31] Shear Stress Transport (SST) turbulence model. Because the nozzle is axisymmetric and the ground is not specified as a boundary condition in the CFD calculation, the resultant steady flow-field is axisymmetric. The flow-field within the first quadrant of the y-z coordinates is obtained with the CFD calculation. After the calculation is complete, only the x-y plane is retained. The computer program that evaluates the prediction model rotates the steady RANS solution about the centerline axis when performing azimuthal integration. The methodology is compatible with other steady RANS solvers and has been demonstrated with the NPARC Alliance Wind-US solver (See Nelson[32] for details).

The geometry of the nozzle is captured by the computational domain. The computational domain is unstructured and contains a region inside the nozzle, a region outside the nozzle upstream of the nozzle exit, and a region for the plume of the jet. The plume region extends 100 nozzle diameters downstream from the nozzle exit and 50 nozzle diameters in the radial direction from the jet centerline. A complete description of the methodology to construct the computational domains used for these types of simulations is found in Miller and Veltin.[33] The nozzle geometry included in the steady RANS simulation is based on the SMC000 nozzle of NASA Glenn Research Center. See Bridges *et al.*[34] for information on the development of the SMC series of nozzles. The nozzle contour is shown in Fig. 2 along with a portion of the computational domain in the jet near-field. The number of grid points in the domain is 205,251 and the number of elements is 204,000.

Boundary conditions are chosen to replicate the experiment of Miles.[7] The 0.3302 m diameter convergent nozzle operates with a fully expanded Mach number of 0.95 and total temperature ratio of 1.00. This results in a fully expanded exit velocity of 301.66 m/s, fully expanded static temperature of 247.7 K, fully expanded speed of sound of 315.5 m/s, and fully expanded density of 1.43 kg/m^3. The characteristic frequency of the jet is 913.6 Hz and the Reynolds number based on the fully expanded jet diameter is 8.944×10^6. A portion of the jet flow-field predicted by FUN3D is shown in Fig. 3. Contours of the streamwise velocity component are shown in the top half plane and contours of turbulent kinetic energy are shown in the lower half plane. The spatially independent variables are normalized by the nozzle exit diameter. Doubling the number of grid points in the streamwise and cross-stream directions yield the same solution. Global residuals of the final CFD solution show reductions of over eight orders of magnitude.

Aeroacoustic Predictions

A free-field calculation is required to validate the prediction method. Since experimental data are not available for this jet operating condition and nozzle diameter in the free-field, the result of the developed acoustic analogy is compared with the SAE ARP876[35] methodology. The SAE ARP876[35] prediction method for single stream shock-associated noise from convergent nozzles at supercritical conditions is included as a prediction module in NASA's ANOPP.[15] The results are presented as lossless Sound Pressure Level (SPL) versus one-third octave band center frequency. In the sideline direction, the agreement between the prediction and SAE ARP876 is satisfactory at all frequencies as shown in Fig. 4.

Predictions of jet noise about the ground plane are now presented. For these comparisons, the nozzle height is 3.89 m and the observer angle is $\psi = 145$ deg. The ground shadow distance is defined as $\sqrt{x_1^2 + x_3^2}$ and is representative of the distance between the nozzle exit and microphone along the ground. The ground shadow distance between the nozzle exit and microphone is $R/D = 69.23$. Figure 5(a) shows the prediction of the jet noise compared with the experiment of Miles.[7] In this comparison the prediction of the jet noise above an acoustically hard surface (ideal) is denoted by a black line with circles, above an asphalt surface (impedance) as a blue line with deltas, and the measurement is denoted by a red line with squares. The y-axis is sound pressure level (SPL) in one-third octave bands and the x-axis is frequency. All following figures use this convention. The ground reflections create select destructive and constructive interference at various frequencies. For example, at 80 Hz the magnitude of the predicted and measured constructive interference agree well. An example of destructive interference occurs at 125 Hz. At frequencies higher than 2500 Hz, the slopes of both the prediction and experiment are approximately the same. However, there is an under-prediction by about two dB through this range.

A second comparison is shown in Fig. 5(b) at $R/D = 69.23$ but the microphone height is lowered to 1.59 m. As the microphone is lowered towards the ground the constructive and destructive interference pattern increases in frequency. This trend matches the analytic solution of the Helmholtz equation with a point source above an infinite flat surface. Both predictions have matching constructive and destructive interference patterns, however these are not aligned with experiment. For example, the first measured destructive interference frequency is near 300 Hz but both predictions are located near 175 to 200 Hz. In addition, the amount of constructive interference in the prediction under-predicts that of experiment. The overall error between the hard-wall prediction and measurement is approximately two to four dB over 1000 Hz and has considerable error approaching 10 dB at lower frequencies. This is consistent with the impedance ground surface prediction that is generally two dB lower over the same frequency ranges.

When the observer is located near the ground, predictions become more challenging. The observer height is set at a height of 0.0061 m. The shadow distance between the microphone and nozzle remains at $R/D = 69.23$. A comparison between the predictions and experiment is shown in Fig. 5(c). The predictions show much more interference relative to experiment, which is probably due to the fact that microphones do not measure pressure at a point but over a small volume of space, and that no air gap exists between the microphone and the ground. The interference pattern is strongly affected by the microphone location, especially when located so close to the ground surface. At low frequencies the prediction shows an extra constructive and destructive pattern relative to the experiment. Overall, in the far-field at $R/D = 69.23$ and at heights high above the ground, the ground effects have been captured by the prediction method.

The ground shadow distance from the nozzle exit to the microphone is set at $R/D = 46.15$ and the microphone heights are set at 3.69, 1.52, and 0.0061 m. Comparisons between predictions and experiment are shown in Fig. 6. At the heights of 3.69 m and 1.52 m in Fig. 6(a) and 6(b) it is shown that both the overall magnitude and peak frequency of the spectrum are within 2 to 4 dB of the measurement, except in the 1.52 m case where there is considerable discrepancy near the first instance of destructive interference. At higher frequencies the prediction is typically 0 to 6 dB lower than experiment. At the ground microphone position the predictions do not compare favorably. The peak frequencies of both predictions are higher than measurement by approximately a few hundred Hz and 2 to 6 dB lower. Once again a constructive interference pattern in the prediction is seen near 30 Hz.

For the final predictions the microphone positions are moved well into the near-field of the jet. Near-field acoustic predictions from jet flows are often very difficult. The shadow distance from the nozzle exit to the microphones is set at $R/D = 23.08$. Figure 7(a) shows the predictions when the microphone height is at 3.89 m. The peak magnitude of the impedance based model agrees very well with experiment and the hard-wall acoustic model is over-predicted by one dB. The peak frequency is approximately 450 Hz. The lowest frequency of the experiment is 40 Hz and is too high to observe any destructive interference. Unfortunately,

the high frequency fall-off of the predictions are larger than the measurement.

A second near-field prediction is shown in Fig. 7(b) where predictions are compared with experiment at $R/D = 23.08$ m and a height of 1.52 m. The predictions are nearly identical except for the slight attenuation due to the ground. Both predictions over-predict the lower frequencies, are within 1 dB of the peak of the experiment, and greatly under-predict the energy above 900 Hz. In the experiment there is very little apparent constructive or destructive interference. A higher fidelity convective wave equation Green's function solver could potentially correct the predictions in terms of the increased fall-off at higher frequencies and also correct for the extra interference at low frequencies.

A final prediction is shown in Fig. 7(c). The microphone height is 0.0061 m and the shadow distance is $R/D = 23.08$ m. This is a difficult position to make an accurate prediction as the observer is on the ground and is within the near-field of the jet. The peak frequency of the hard-wall prediction is 100 Hz higher than the experiment and the impedance peak frequency is 200 Hz lower than the experiment. The attenuation between the hard-wall prediction and the impedance prediction is much larger than previously seen. Unfortunately, the prediction using a ground surface with realistic impedance greatly under-predicts the measurement. It should be noted how extremely sensitive to the microphone position and ground impedance the predictions are. Even a slight change of microphone height of 0.001 m near the ground can greatly influence the constructive-destructive interference patterns. Small changes in the impedance can also greatly change the predicted values. In the near-field of the jet, roughness or small irregularities on the ground surface can greatly change the experimental result. This causes obvious difficulty when predictions are assumed about a perfectly flat surface and are amplified in the near-field of the jet. Overall, the predictions are satisfactory considering the sensitivity of the problem, measurement, and conducted in the near-field at a jet emission angle that is relatively less understood than the sideline.

Conclusion

An acoustic analogy is formulated and the arguments are the vector Green's function of the LEE and equivalent sources. The latter involves the two-point cross-correlation of the turbulent velocity fluctuations and scaling terms based on a steady RANS solution. The vector Green's function of the LEE is written in relation to Lilley's[4] equation, which is approximated with matched asymptotic solutions about the Green's function of the convective Helmholtz equation. The Green's function of the Helmholtz equation is found analytically for the infinite flat plane. Large savings have been made in terms of computational cost with a minimal loss of accuracy relative to finding the full solution of the vector Green's function of the LEE. The new model has been exercised and compared with the experiment of Miles.[7] The predictions are shown to capture jet noise ground effects that are characterized by constructive and destructive interference patterns in the mid- and far-field and capture overall trends in the near-field. However, there are discrepancies with respect to measurement of the magnitudes and frequencies of select constructive and destructive interference patterns.

The choice to study ground effects is due to the availability of experimental data and the ease of finding the appropriate Green's function. This model formulation allows a multitude of well-known Green's function solvers to account for scattering of jet mixing noise as long as the plume is not highly influenced by the scattering surface. The problem has been greatly simplified by relating the vector Green's function of the LEE to the Green's function of the convective Helmholtz equation while still retaining the benefits of Lilley's equation that accounts for jet shear layer refraction and amplification.

Acknowledgments

This work is inspired by the creative ideas of Prof. Feri Farassat and Dr. Marvin E. Goldstein of the National Aeronautics and Space Administration (NASA), Boeing/A. D. Welliver Prof. Philip J. Morris, and Robert O. Lawton Distinguished Prof. C. K. W. Tam. Dr. Jeffrey H. Miles of the NASA Glenn Research Center at Lewis Field is gratefully acknowledged for the use of his experimental data. The data were used with permission. The author is grateful for continuous support from the NASA Fundamental Aeronautics Program High Speed Project.

References

[1]Morris, P. J. and Farassat, F., "Acoustic Analogy and Alternative Theories for Jet Noise Prediction," *AIAA Journal*, Vol. 40, No. 4, 2002, pp. 671–680.

[2]Tam, C. K. W. and Auriault, L., "Jet Mixing Noise from Fine-Scale Turbulence," *AIAA Journal*, Vol. 37, No. 2, 1999, pp. 145–153.

[3]Morris, P. J. and Boluriaan, S., "The Prediction of Jet Noise From CFD Data," *10th AIAA/CEAS Aeroacoustics Conference, Manchester, Great Britain, May 10-12, AIAA Paper 2004-2977*, 2004.

[4]Lilley, G. M., "On the Noise from Jets," *AGARD Conference Proceedings In Noise Mechanisms*, Vol. 13, 1974, pp. 1–11.

[5]Delany, M. E. and Bazley, E. N., "Acoustical Properties of Fibrous Absorbent Materials," *Applied Acoustics*, Vol. 3, 1970, pp. 105–116.

[6]Banos, A., "Dipole Radiation in the Presence of a Conducting Half-Space," *Oxford, New York, Pergamon Press*, 1966.

[7]Miles, J. H., "Analysis of Ground Reflection of Jet Noise Obtained with Various Microphone Arrays over an Asphalt Surface," *NASA Technical Memorandum X-71696*, 1975.

[8]Seiner, J., Jansen, B., and Ukeiley, L., "Acoustic Fly-Over Studies of F/A-18 E/F Aircraft During FCLP Mission," *9th AIAA/CEAS Aeroacoustics Conference, Hilton Head, S.C., May 12-14, AIAA Paper 2003-3330*, 2003.

[9]Butzel, L. M., "Prediction of Jet Exhaust Noise on Airframe Surfaces during Low-Speed Flight," *Journal of Aircraft*, Vol. 19, No. 12, 1982, pp. 1038–1044.

[10]Schlinker, R., Liljenberg, S., Polak, D., Post, K., Chipman, C., and Stern, A., "Supersonic Jet Noise Characteristics and Propagation: Engine and Model Scale," *13th AIAA/CEAS Aeroacoustics Conference, Rome Italy, AIAA 2007-3623*, 2007.

[11]Pao, S., Wenzel, A., and Oncley, P., "Prediction of Ground Effects on Aircraft Noise," NASA Technical Paper 1104, 1978.

[12]Huber, J. and Sogeti, S., "Jet Noise Assessment and Sensitivity at Aircraft Level," *13th AIAA/CEAS Aeroacoustics Conference (28th AIAA Aeroacoustics Conference), Rome, Italy, May 21-23, AIAA Paper 2007-3728*, 2007.

[13]Illston, L. W., Angel, R. G. A., Patience, D. E., and Burns, R. E., "Assessment Methods for Near Field Noise and Ground Erosion," *AIAA International Powered Lift Conference, AIAA Paper 1993-4870*, 1993, pp. 208–219.

[14]Harper-Bourne, M., "Predicting the Jet Near-Field Noise of Combat Aircraft," *RTO AVT Symposium on Aging Mechanisms and Control, Oct. 8-11*, 2001.

[15]Zorumski, W. E., "Aircraft Noise Prediction Program. Theoretical Manual. Parts 1 and 2," NASA TM 83199, 1982.

[16]Chien, C. and Soroka, W., "Sound Propagation Along an Impedance Plane," *Journal of Sound and Vibration*, Vol. 43, No. 1, 1975, pp. 9–20.

[17]McLaughlin, D. K., Kuo, C., and Papamoschou, D., "Experiments on the Effect of Ground Reflections on Supersonic Jet Noise," *46th AIAA Aerospace Sciences Meeting and Exhibit, Reno, Nevada, Jan. 7-10, AIAA Paper 2008-22*, 2008.

[18]Ribner, H. S., "The Generation of Sound by Turbulent Jets," *Advances in Applied Mechanics*, Vol. 8, 1964, pp. 104–182.

[19]Tam, C. K. W. and Auriault, L., "Mean Flow Refraction Effects on Sound Radiated from Localized Sources in a Jet," *Journal of Fluid Mechanics*, Vol. 370, 1998, pp. 149–174.

[20]Raizada, N., "Numerical Prediction of Noise from High Speed Subsonic Jets using an Acoustic Analogy," *M.S. Thesis The Pennsylvania State University*, December 2005.

[21]Goldstein, M. E., "Aeroacoustics," McGraw-Hill, New York, 1976.

[22]Goldstein, M. E., "The Low Frequency Sound from Multipole Sources in Axisymmetric Shear Flows, with Applications to Jet Noise," *Journal of Fluid Mechanics*, Vol. 70, No. 3, 1975, pp. 595–604.

[23]Goldstein, M. E., "The Low Frequency Sound from Multipole Sources in Axisymmetric Shear Flows - Part II," *Journal of Fluid Mechanics*, Vol. 75, No. 1, 1976, pp. 17–29.

[24]Balsa, T. F., Gliebe, P. R., Kantola, R. A., Mani, R., and Stringas, E. J., "High Velocity Jet Noise Source Location and Reduction. Task 2. Theoretical Developments and Basic Experiments," *Defense Technical Information Center*, 1978.

[25]Tinetti, A. F. and Dunn, M. H., "The Fast Scattering Code (FSC): Validation Studies and Program Guidelines," *NASA/CR-2011-217158*, 2011.

[26]Katsikadelis, J. T., "Boundary Elements Theory and Applications," *Elsevier, Kidlington, Oxford, United Kingdom*, 2002.

[27]Liu, Y. J., "Fast Multipole Boundary Element Method - Theory and Applications in Engineering," Cambridge University Press, Cambridge, 2009.

[28]Attenborough, K. and Ver, I. L., *Sound-Absorbing Materials and Sound Absorbers in Noise and Vibration Control Engineering: Principles and Applications*, John Wiley & Sons Inc., Hoboken, N.J. USA, 2nd ed., 2007.

[29]Anderson, W. K. and Bonhaus, D. L., "An Implicit Upwind Algorithm for Computing Turbulent Flows on Unstructured Grids," *Computers and Fluids*, Vol. 23, No. 1, 1994, pp. 1–22.

[30]Nielsen, E. J., *Aerodynamic Design Sensitivities on an Unstructured Mesh using the Navier-Stokes Equations and a Discrete Adjoint Formulation*, Ph.D. thesis, Virginia Polytechnic Institute and State University, 1998.

[31]Menter, F. R., "Two-Equation Eddy-Viscosity Turbulence Models for Engineering Applications," *AIAA Journal*, Vol. 32, No. 8, 1994, pp. 1598–1605.

[32]Nelson, C. and Power, G., "The NPARC Alliance Flow Simulation System," AIAA Paper 2001-0594, 2001.

[33]Miller, S. A. E. and Veltin, J., "Assessment of Computational Fluid Dynamics for Supersonic Shock Containing Jets," *AIAA Journal*, Vol. 47, No. 11, 2009, pp. 2738 – 2746.

[34]Bridges, J. and Brown, C. A., "Validation of the Small Hot Jet Acoustic Rig for Aeroacoustic Research," *11th AIAA/CEAS Aeroacoustics Conference, Monterey, California, 23 - 25 May, AIAA Paper 2005-2846*, 2005.

[35]SAE International, *SAE ARP876, Revision D. Gas Turbine Jet Exhaust Noise Prediction*, SAE International, Warrendale, PA, 1994.

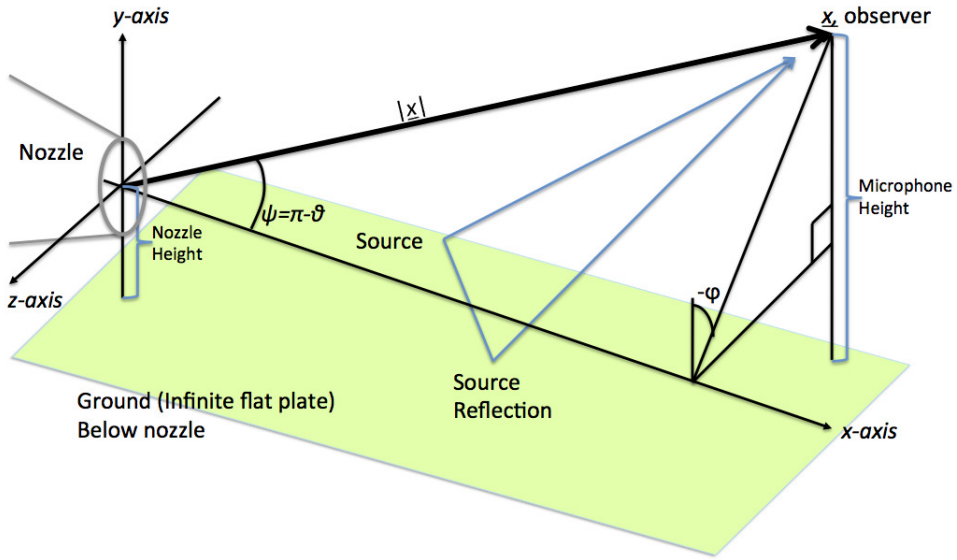

Figure 1. The coordinate system showing the nozzle, the ground plane, and the observer. The positive y-axis points away from the ground below the nozzle. The origin of the coordinate system resides at the center of the nozzle exit.

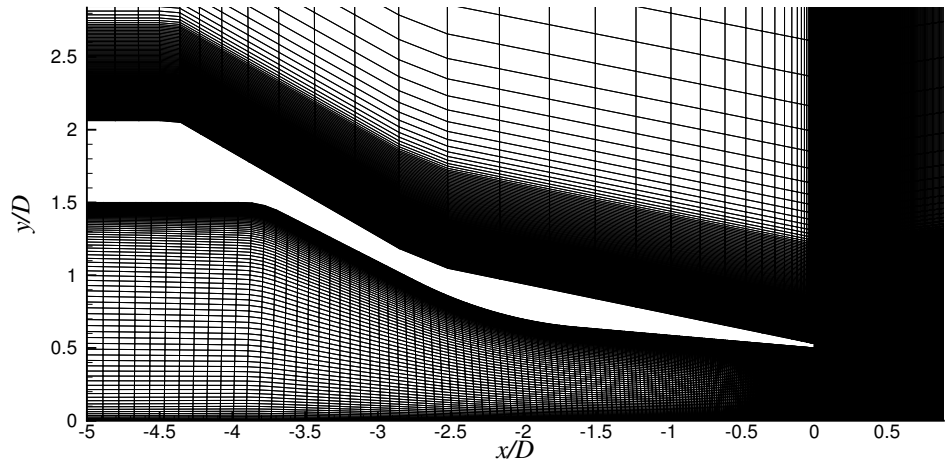

Figure 2. A slice of the computational domain showing the convergent contoured nozzle. The x- and y-axis have been normalized by the nozzle exit diameter. The nozzle geometry corresponds to the NASA Glenn Research Center SMC000 nozzle.

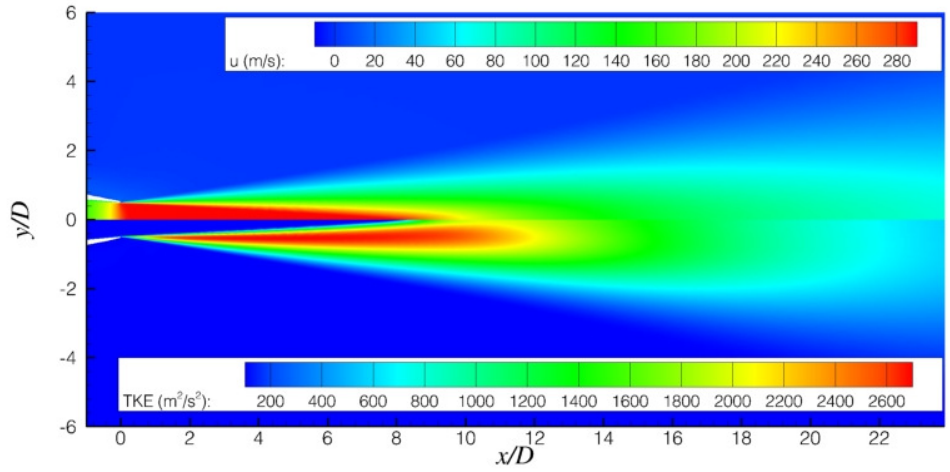

Figure 3. Contour maps of the steady RANS solution closed by the Menter[31] SST turbulence model. The coordinates are normalized by the nozzle diameter. In the top half plane contours of the streamwise velocity component, u m/s, are shown. In the bottom half plane contours of turbulent kinetic energy, TKE (m^2/s^2), are shown.

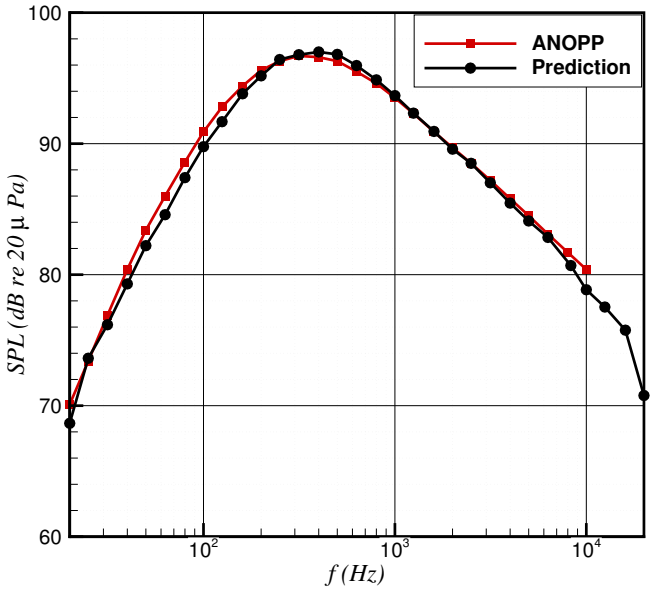

Figure 4. Free-field predictions of the SAE ARP876[35] method contained within the Aircraft Noise Prediction Program (ANOPP) and the developed acoustic analogy. The jet conditions are $M_j = 0.95$, $TTR = 1.00$, $D = 0.3302$ m, $R/D = 100$, $\psi = 145$ degrees (inlet angle), and azimuthal angle $\phi = 90$ degrees.

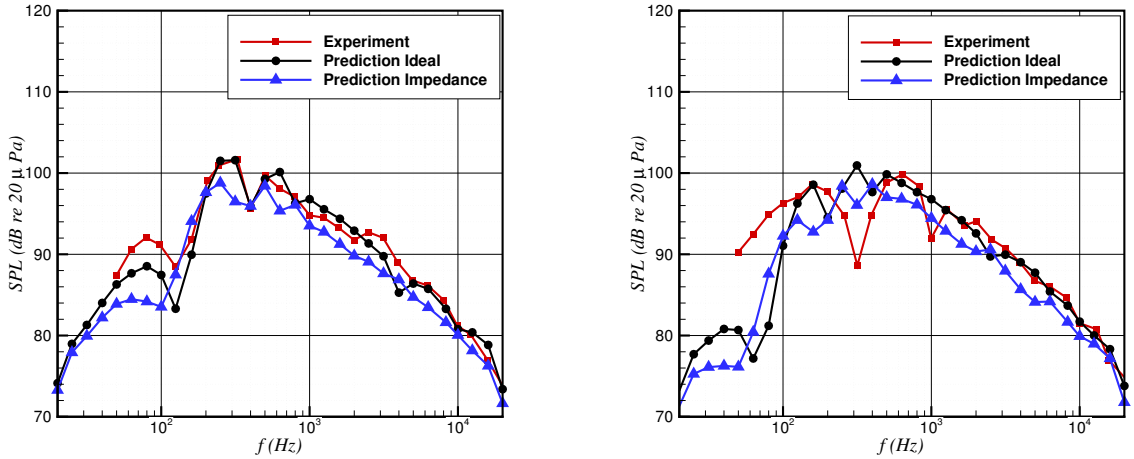

(a)

(b)

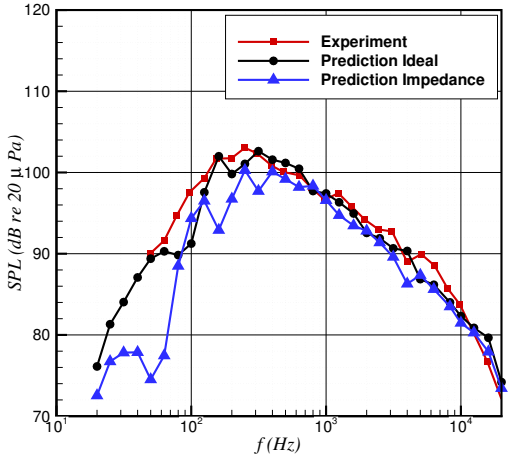

(c)

Figure 5. Ground shadow distance $R/D = 69.2308$ and microphone heights a) 3.89 m, b) 1.52 m, and c) 0.0061 m (ground).

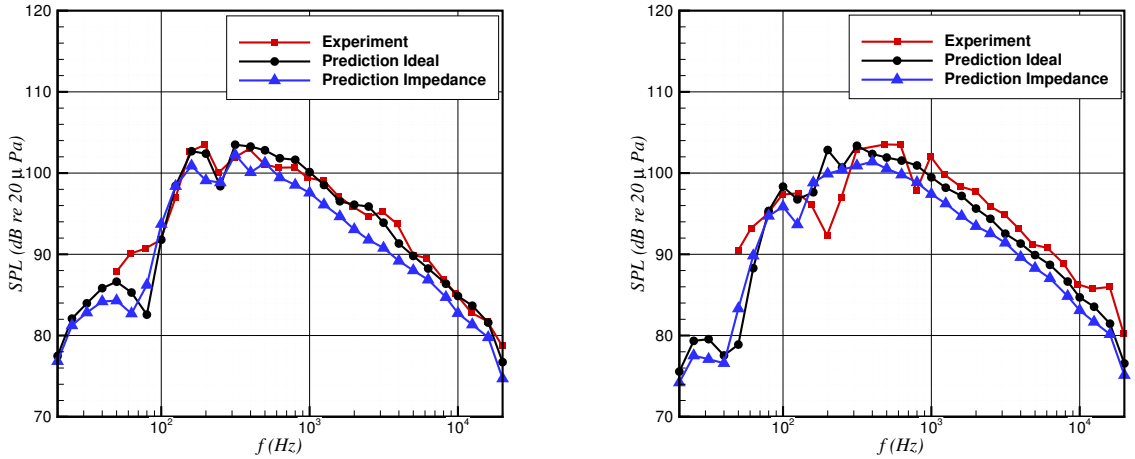

(a)

(b)

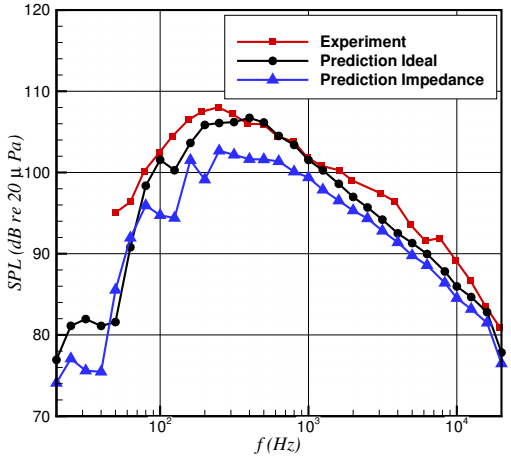

(c)

Figure 6. Ground shadow distance $R/D = 46.1538$ and microphone heights a) 3.89 m, b) 1.52 m, and c) 0.0061 m (ground).

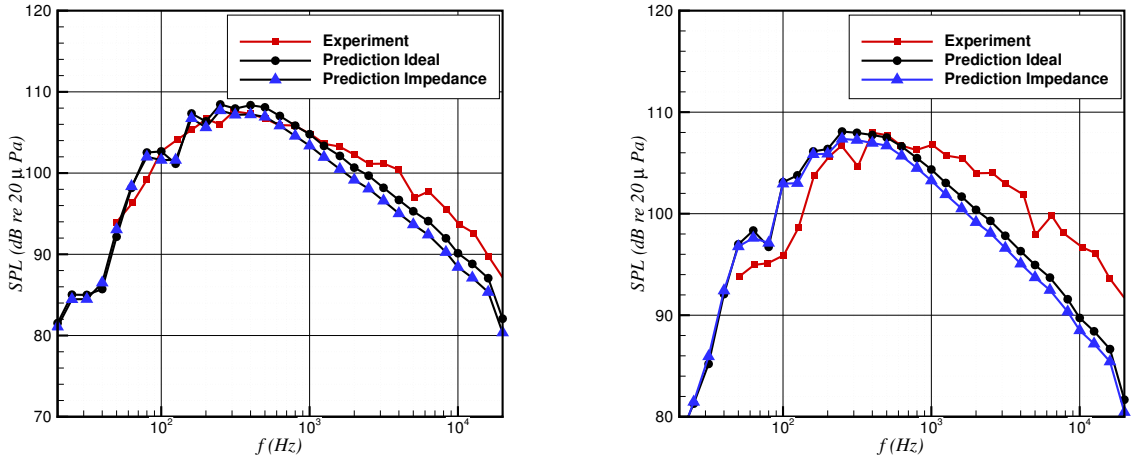

(a)

(b)

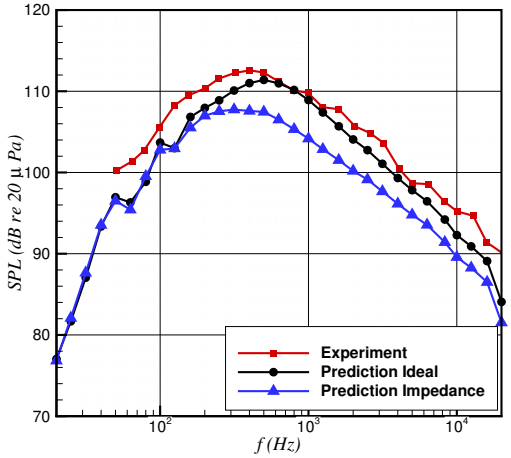

(c)

Figure 7. Ground shadow distance $R/D = 23.0769$ and microphone heights a) 3.89 m, b) 1.52 m, and c) 0.0061 m (ground).